Journal of Materials Chemistry A

Accepted Manuscript

ROYAL SOCIETY OF CHEMISTRY

www.rsc.org/materialsA

Facile and scalable production of three-dimensional spherical carbonized bacterial cellulose/graphene nanocomposites with honeycomb-like surface pattern as potential superior absorbents

Yizao Wan [a,b], Fangshan Zhang [b], Chunzhi Li [a], Guangyao Xiong [a,*], Yong Zhu [c], Honglin Luo [a,b,*]

[a] *Institute for Biomaterials and Transportation, East China Jiaotong University, Nanchang 330013, China*

[b] *School of Materials Science and Engineering, Tianjin University, Tianjin 300072, China*

[c] *School of Chemical Engineering, Tianjin University, Tianjin 300072, China*

Abstract

Frequent contamination of water by oils and organic solvents necessitates efficient and low cost absorbents. Here, for the first time, a novel nanocomposite of sphere-like carbonized bacterial cellulose (SCBC) and graphene (GE) with honeycomb-like surface morphology and three-dimensional (3D) interconnected porous structure was synthesized via a facile and scalable one-pot in situ biosynthesis route under agitated culture conditions followed by carbonization. The as-prepared SCBC/GE nanocomposite was characterized by SEM, TEM, XRD, FTIR, Raman, wettability, and absorption capacity measurements. SEM images reveal that the SCBC/GE nanocomposite exhibits honeycomb-like surface pattern consisting of ridges and large cavities with an average diameter of around 97 μm. Furthermore, the SCBC/GE

nanocomposite has high porosity, large specific surface area, strong hydrophobicity, and good elasticity. Importantly, it shows superior absorption capacities for a wide range of oils and organic solvents (the maximum value reaches 457 times of its own weight), higher than any other CNF-based aerogels reported so far, thus having the potential to be used in the field of environmental protection. Additionally, the underlying absorption mechanisms for oil and organic solvents have been explored.

1. Introduction

Dealing with water pollution from oil spillage and chemical leakage with absorbents is considered to be the most promising strategy although other methods, such as booms and skimmers, dispersants, and combustion, are still being used.[1-4] In this context, absorbents, in the form of foam and powder,[5-7] with high absorption capacity, fast absorption kinetics, excellent selectivity and recyclability, and controllable hydrophobicity are highly demanded due to the increasing water pollution from the crude oil, petroleum products, and toxic organic solvents.[8-10] Traditional absorbents such as activated carbon,[11, 12] expanded perlite,[5, 13] and zeolites [14] have been developed to remove the aforementioned pollutants.[9] However, the drawbacks of those absorbents including poor efficiency and/or incidental contamination arising from the cleanup procedure[2, 15] encourage researchers to explore better alternatives. Up to date, numerous new absorbents have been investigated, such as nanocellulose aerogels,[16, 17] magnetic foams,[18] polymer sponges,[19] metal oxide nanowire membranes,[20] carbon monoliths,[21] graphene (GE)-based materials,[8, 22] and carbon nanofibers (CNFs).[23] Among these absorbents under investigation, three-dimensional (3D) porous carbon-based materials, usually in the form of sponge or foam, such as carbon nanotubes (CNTs),[24-26] GE,[8, 27, 28] and CNFs,[4, 23, 29] have received tremendous attention in light of their low apparent density, high porosity, large specific surface area, intrinsic surface hydrophobicity and superwettability for organic solvents and oils, and environmental friendliness.[10] For instance, a CNT sponge could absorb various solvents and oils with excellent selectivity, recyclability, and absorption

capacities up to 180 times of their own weight.[25] Very recently, the 3D macroporous CNT solid material prepared by Ozden et al. absorbed ~120 times of its own weight of oil.[26] The spongy GE reported by Bi et al. showed highly efficient absorption of not only petroleum products and fats, but also toxic solvents such as toluene and chloroform (up to 86 times of its own weight).[8] These CNTs and GE, in the above-highlighted works were generally produced by sophisticated chemical vapor deposition (CVD), and multistep exfoliation and reduction methods, respectively. Alternatively, Yu and co-workers have reported the production of CNF aerogels from bacterial cellulose (BC) hydrogels by static culture, which produced gelatinous membrane of cellulose and the resultant carbonized materials in the form of sheet presented good performance in absorption of oils and organic solvents (absorb up to 300 times of their weight in oils or organic liquids).[29] Apart from membrane, sphere-shaped BC can be produced by agitated fermentation.[30, 31] The sphere-like carbonized BC (denoted as SCBC hereinafter) is expected to show additional advantages of high absorption capacities due to its larger surface area as compared to the shape of sheets and easy operation for spreading on spills to collect oils like sawdust. Therefore, replacement of sawdust with SCBC spheres will not change the traditional process, which will be beneficial to its large-scale applications.

Besides single carbonaceous materials, hybrids or composites consisting of various carbon-based materials have been developed to make full use of their advantages for absorption of organic pollutants.[32-34] A recent study demonstrated that the hybrid aerogels constructed with cell walls of giant GE sheets and CNTs ribs

possessed ultrahigh oil-absorption capacities of 215-743 times of their own weights.[35] It is expected that the rational hybridization of SCBC with GE may sustain the 3D porous structure and huge surface area and the excellent hydrophobicity and mechanical properties of GE. Furthermore, the GE serving as skeleton will resist the shrinkage and collapse of spherical BC (denoted as SBC) during its carbonization, thus leading to extraordinarily high surface area of the resultant SCBC/GE nanocomposite aerogels.

Recently, nanocomposites consisting of BC and GE or graphene oxide (GO) have been prepared, mainly by mixing BC fragments with GE or GO,[36, 37] which destroyed the 3D interconnected network structure of pristine BC. What is more, these cellulose and GO-containing aerogels do not show oleophilicity due to large amounts of surface hydroxyl groups on BC and carboxyl groups on GO when surface modification is not conducted. In order to sustain the intrinsic 3D interconnected porous structure of BC, in our previous work, the *in situ* biosynthesis route was adopted and GE[38] and GO[39] were uniformly distributed in BC network. However, the existence of GE- or GO-deplete zones was inevitable when the nanocomposite pellicles became thick (> 3 mm). In order to tackle these problems aforementioned, the agitated culture method should be a good solution. Moreover, carbonization of SBC is also necessary to obtain hydrophobic SCBC.

Herein, for the first time, sphere-like nanocomposite hydrogels of SBC and GE (SBC/GE) with honeycomb-like surface pattern and three-dimensionally connected porous network structure have been successfully synthesized via a facile and scalable

one-pot *in situ* biosynthesis route under agitated culture conditions, which was believed to be the most suitable technique for economical large-scale production of BC as compared to static culture. Furthermore, under agitated culture conditions, the cellulose is synthesized in deep media,[31] thus uniformly distributed GE throughout SBC/GE nanocomposite can be achieved. The SBC/GE nanocomposite was then pyrolyzed under argon atmosphere leading to sphere-like SCBC/GE nanocomposite. The SCBC/GE has a novel honeycomb-like surface pattern and exhibits extraordinarily large specific surface area and, in particular, the SCBC/GE without any surface modification demonstrates superior absorption capacities for a wide range of oils and organic solvents with a maximum absorption capacity up to 457 times of its own weight, making it promising as a superior all-carbon absorbent for oils and organic solvents. The extraordinary high absorption capacities are mainly ascribed to its unique honeycomb-like surface pattern.

2. Materials and methods

2.1 Preparation of SBC and SBC/GE hydrogels via in situ biosynthesis

In accordance to our previous work,[40, 41] the bacterial strain, *Acetobacter xylinum* X-2, was used to produce SBC and SBC/GE hydrogels. The culture medium was sterilized at 121 °C for 30 min prior to use. The medium for the pristine SBC was composed of 2.5% (w/v) glucose, 0.75% (w/v) yeast extract, 1% (w/v) tryptone, and 1% (w/v) disodium phosphate (Na_2HPO_4), and the pH was adjusted to 4.5 by acetic acid. To prepare the SBC/GE nanocomposite hydrogel, a GE-dispersed culture medium was prepared. Typically, 2 mL GE suspension (monolayer, purity ≥ 99.4 wt%,

concentration of suspension = 50 mg/L, Institute of Coal Chemistry, Chinese Academy Sciences, China) was added to 30 mL culture medium aforementioned, followed by intense stirring for 60 min. The incubation was conducted on a rotary shaker with a rotation speed of 160 rpm. After 2 days incubation at 30°C, the spherical SBC/GE hydrogel was collected. For comparison purposes, gelatinous membranes of BC and BC/GE were also prepared as control groups following the same procedures reported in literature.[38] The harvested products were purified by soaking in deionized water at 90 °C for 2 h, boiled in a 0.5 M NaOH solution for 15 min, and then washed several times with deionized water until they reached a neutral pH. The water in the hydrogels was removed through solvent exchange with tertiary butanol followed by successive freeze-drying at -20 °C for 12 h and -54 °C for 24 h, resulting in BC, SBC, BC/GE, and SBC/GE aerogels.

2.2 Preparation of spherical SCBC and SCBC/GE nanocomposite aerogels

The freeze-dried samples were carbonized at 800 °C for 2 h in a tubular furnace following the heating and cooling procedures shown in Fig. S1 in the Supporting Information.

2.3 Characterization

The photos of SBC spheres were taken by a digital camera (Canon N118). For SEM observation, the aerogel spheres were sputtered with gold and evaluated by a field-emission scanning electron microscope (FE-SEM, Hitachi, S-4800). For fiber diameter and cavity size measurements, 100 randomly selected fibers and cavities were measured using an Image J2x software (National Institutes of Health, USA).

X-ray diffraction (XRD) was carried out by a Rigaku D/max 2500 to examine the crystalline structure. The surface properties of aerogels were investigated using a Fourier transform infrared spectrometer (FTIR, Nicolet MAGNA-560). The spectra were recorded in a spectral range of 4000-400 cm^{-1} with a resolution of 4 cm^{-1}. Raman spectra were recorded by an RM2000 spectrometer (Renishaw Co.).

Contact angle measurements were conducted using the sessile drop method on a DropMaster 300 liquid/solid interface analyzer (Japan) equipped with a CCD camera using deionized water as the medium at room temperature. The samples for contact angle measurements were prepared by pressing spherical samples into flattened ones. A microliter water droplet was dropped onto the sample surfaces and the contact angle was measured 10 s afterwards at room temperature. The captured images of sessile drops were analyzed using drop-shape analysis SCA20 software. All contact angles were determined by averaging values measured at five different positions on each sample surface.

The compressive tests of SCBC and SCBC/GE were performed by using the micro electromagnetic fatigue testing machine (MUF-1050, Tianjin Care Measure & Control Co., Ltd., Tianjin, China). The strain rate was maintained at 0.2 mm min^{-1}.

The Brunauer–Emett–Teller (BET) surface area was evaluated from nitrogen adsorption isotherms at 77 K using a surface area analyzer (Quantachrome, USA). The density was determined by measuring the weight and volume of each individual aerogel. The weight of an aerogel sphere (W_0) was determined by measuring 100 spheres by an analytical balance (readability 0.1 mg) and the volume (V_e) of an

aerogel sphere was obtained by measuring the volume saturated with ethanol of a sphere. Therefore, the density (ρ_0) and porosity (P) of an aerogel were obtained by Equations (1) and (2), respectively.

$$\rho_0 = \frac{W_0}{V_e} \quad (1)$$

$$P(\%) = \frac{W_e - W_0}{\rho V_e} \times 100\% \quad (2)$$

where ρ is the density of ethanol and W_e is the weight of an ethanol-saturated sphere. All measurements were repeated at least 10 times.

2.4 Absorption capacity measurements

Liquid absorption capacities for a series of commercial oils and organic solvents were evaluated following previously reported methods.[9, 21, 22] Typically, aerogels were weighed and immersed into different kinds of oils or organic solvents until the aerogels were completely filled with the organic liquid, which took a few seconds depending on the samples and liquids, then taken out with a tweezer, and immediately weighed again. The measurement was done quickly at ambient temperature to avoid evaporation of the absorbed liquids. The absorption capacity expressed by weight gain, wt%, is defined as the weight of oils or organic solvents absorbed per the unit weight of the initial aerogel, namely the weight ratio of the absorbed oil/solvent to the aerogel.

3. Results and discussion

3.1 Morphology and structure

Low-magnification SEM images of the surfaces of various aerogels are shown in Fig.

1. Unlike BC synthesized under static conditions that shows smooth surface (Fig. 1a), SBC shows unique honeycomb-like surface pattern (Fig. 1b) which consists of numerous ridges and large cavities with an average diameter of 107 μm (Fig. 2S). The open honeycomb-like surface is expected to increase the specific surface area and porosity of the resultant aerogels. Although how the SBC is formed remains elusive, some researchers believe that it is the continuous shear force generated during agitation that causes the cellulose ribbons to intertwine with each other to form the spherical structure.[30, 31] Notably, after pyrolysis, the obtained CBC and SCBC still keep the morphological features of BC and SBC (Fig. 1c and d), respectively, although obvious volume shrinkage is noted for all samples (Fig. S3). Furthermore, the incorporation of GE does not change the surface pattern of SBC and SCBC (Fig. 1e and f). However, the average cavity sizes of SCBC and SCBC/GE exhibit slight differences (Fig. 2S). High-magnification SEM images reveal that SBC has a similar 3D porous interconnected fibrous structure to BC (Fig. 2a and c) while twisted individual nanofibers are observed for both CBC and SCBC due to evaporation of some volatile species during calcination (Fig. 2b and d). Fig. 2e and f clearly shows the existence of GE nanosheets embedded in the network of SBC and SCBC. Note that SCBC/GE (Fig. 2f) sustains the morphological features of SBC/GE (Fig. 2e), showing a 3D interconnected porous structure. In other words, the 3D network of the nanofibrous aerogel can survive well even after pyrolysis at a high temperature. The fiber diameter distribution shown in Fig. S4 reveals that the average diameter of nanofibers decreases substantially from around 50 nm (for BC and SBC) to around 20

nm (for CBC and SCBC). Note that the incorporation of GE leads to decreased fiber diameter (SCBC vs. SCBC/GE; SBC vs. SBC/GE). The porous interconnected fibrous structure, decreased fiber diameter due to the pyrolysis and incorporation of GE, entangled GE nanosheets with BC and CBC nanofibers, and amorphous structure of individual CNFs can also be observed from TEM and HRTEM images (Fig. S5 and insets). The entanglement between GE nanosheets and cellulose nanofibers or CNFs is important to the loading capacity of the GE-contained nanocomposites.

XRD results (Fig. 3) demonstrate that three peaks corresponding to $(1\bar{1}0)$, (110), and (200) planes of cellulose I [38, 42] are observed in the spectra of BC, SBC, and SBC/GE. The absence of the peaks assigned to carbon indicates that the CNFs in CBC, SCBC, and SCBC/GE have amorphous structure, in agreement with the findings from TEM (Fig. S5). The absence of GE peaks in the spectra of SBC/GE and SCBC/GE is likely due to the single-layer GE that does not show apparent diffraction peak at around $2\theta = 13.7°$. [43, 44] Another possible reason is related to the uniform distribution of GE in the network of interconnected CNFs, in agreement with previously reported results. [38, 45, 46] Raman analysis demonstrates that there is no difference in D and G bands (Fig. S6), indicating that the fermentation manner and incorporation of GE have no effect on the structure of CNFs in CBC, SCBC, and SCBC/GE.

FTIR spectra (Fig. 4) demonstrate the presence of hydrophilic functional groups including C=O, C-O, and -OH on the surface of BC, SBC, and SBC/GE,[47], while, after pyrolysis, these groups are remarkably weakened or disappear in the resultant

CBC, SCBC, and SCBC/GE. This confirms the hydrophobic nature of these carbon-based aerogels.

3.2 Physical and mechanical properties

To evaluate the hydrophobicity of the aerogels, the contact angles were measured (Fig. 5). Note that there is no significant difference in the contact angles between BC (44.7^{o}) and SBC (43.5^{o}), indicating fermentation manner does not significantly affect the wettability of BC materials. Similarly, the difference between CBC (116.8^{o}) and SCBC (117.7^{o}) is not significant neither. However, the incorporation of GE in SCBC results in significantly increased contact angles ($p < 0.05$, SCBC/GE *vs*. SCBC). Fig. 5 also reveals that pyrolysis causes extraordinarily larger contact angles due to the removal of hydrophilic functional groups, as evidenced by the FTIR results.

Porosity measurements (Fig. 6) reveal that there is no significant difference in porosity between CBC and SCBC ($p > 0.05$). The higher porosity of SCBC/GE than SCBC ($p < 0.05$) is likely related to the skeleton role of GE which helps to resist the volume shrinkage during pyrolysis. The specific surface area follows the similar changing pattern of porosity (Fig. 7). As expected, SCBC/GE shows much larger specific surface area (514.0 $m^2 g^{-1}$) in comparison to SCBC (229.6 $m^2 g^{-1}$) due to the large surface area of GE nanosheets, the effective role of GE nanosheets in resisting the shrinkage during pyrolysis, and the smaller CNF fiber diameter. The specific surface area of SCBC/GE is much higher than that of nitrogen-doped GE framework (280 $m^2 g^{-1}$) [48] and is comparable to that of CNF aerogels (547 $m^2 g^{-1}$).[4]

Mechanical performance is an important parameter of the absorbents. We

conducted compression tests on SCBC and SCBC/GE to assist this. We failed to calculate the stress due to the difficulty in obtaining the effective cross-sectional area of these spherical samples; rather, we could compare their compressive responses by selecting some spheres with almost identical diameters for SCBC and SCBC/GE. Fig. 8 demonstrates that SCBC/GE shows a higher load (0.8 N) than that of SCBC (0.6 N) at a large compressive ratio of 90%. This finding indicates that the incorporation of GE greatly increases the strength of SCBC, due to the highly dispersed GE nanosheets in the network of SCBC and the entanglement between GE nanosheets and CNFs, as revealed by SEM and TEM. Similar to previous reports,[49, 50] three distinct stages are observed during the loading process, including an initial linear region, a gradually increasing slope and finally a quick increase in the stress. It should be pointed out that SCBC and SCBC/GE display a nearly complete recovery after 90% compression ratio, indicating good elasticity, which is consistent with that observed by Yu and co-workers.[29]

3.3 Absorption capacities

The good hydrophobicity, high porosity, and mechanical stability make the SCBC/GE an excellent absorbent for oils and organic solvents. To demonstrate the absorption capacities of the spherical SCBC/GE, we followed the methodology reported by Yu and co-workers.[4] First, as shown in Fig. 9a-d and Movie S1 (Supporting Information), the hexane (dyed with Sudan III) floating on the water can be absorbed quickly and completely within a minute. Next, as shown in Fig. 9e-h and Movie S2 (Supporting Information), we tested the absorption capacity of SCBC/GE for a high-density

organic solvent, like phenoxin, that sank to the bottom of the beaker and aggregated while SCBC/GE was floating on the water. A tweezer was used to force the aerogel to approach the phenoxin. We found that the phenoxin (dyed with Sudan III) was rapidly absorbed by the SCBC/GE aerogel.

In order to quantitatively examine the absorption efficiency of SCBC/GE, we measured the absorption capacities for various oils (such as diesel oil and pump oil) and organic solvents (such as DMF, hexane, cyclohexane, and toluene). For comparison purposes, CBC and SCBC were also measured. As shown in Fig. 9i, the absorption capacities of SCBC are significantly higher than those of CBC for all liquids tested in this work and SCBC/GE shows the highest absorption capacities among three carbonaceous aerogels. Notably, SCBC/GE displays extraordinarily high absorption capacities to numerous oils and organic solvents. The absorption capacities range from 243 to 457 times of its own weight. Compared to other all-carbon absorbents reported in literature, for example, BC-derived CNFs (106-312),[29] hybrid foam of GE/CNT (80–130),[32] CNT sponges (80–180),[25] GE aerogels (120-250)[50] and nitrogen doped GE framework (200–600),[48] the spherical SCBC/GE aerogel prepared in this work possesses superior absorption capacities. To our knowledge, this is the best absorption performance reported for any CNF-based aerogels to date. More importantly, the fabrication of this unique spherical aerogel is simpler and can be more easily scaled up than that of GE-based or CNT-based absorbent counterparts.

It has been well documented that the absorption capacity is dependent on many physicochemical parameters of absorbents and absorbates including density, surface

tension, viscosity, polarity, hydrophobicity, porosity, and pore size.[15, 21] It is believed that the existence of macropores favors accommodation of absorbates. In general, BC sponges synthesized under static conditions have 3D interconnected and hierarchical pore structure. However, they lack the macropores larger than 20 μm.[51] We believe that the honeycomb-like surface pattern consisting of large cavities (97 μm in average) and ridges makes a significant contribution to the high absorption quantity of SCBC/GE. We believe that the unique honeycomb-like surface of SCBC/GE improves the absorption capacities through the following mechanisms. (i) The honeycomb-like surface pattern increases specific surface area and porosity as compared to CBC. (ii) The interconnected cavities form a network that provides more sufficient space and active sites enabling the absorbates to access all the surfaces of porous spheres, improving the efficiency of liquid diffusion and the hydrophobic interactions between absorbates and carbon. (iii) More importantly, as illustrated in Fig. 10, the ridges act to cut the absorbates (bulky absorbates become small ones) and thus facilitate dispersive interactions between hydrophobic carbon and hydrophobic absorbate molecules,[21] while the cavities act to catch the absorbates and then assign them to the pore channels underneath. Therefore, the open cavities and distinct ridges allow fast access and diffusion of absorbate molecules, leading to high absorption capacities to oils and organic solvents. Although further investigation is required to verify the mechanisms, the present study demonstrates that the unique spherical SCBC/GE aerogel shows promise as a new superior absorbent.

4. Conclusion

A novel all-carbon aerogel based on spherical carbonized bacterial cellulose and GE (SCBC/GE) has been successfully fabricated. The spherical SCBC/GE nanocomposite aerogel displays honeycomb-like surface pattern consisting of ridges and large cavities and sustains the 3D porous interconnected structure of pristine BC. The SCBC/GE aerogel with this unique structure exhibits good elasticity and hydrophobicity and, more importantly, it shows superior absorption capacities, which are significantly higher than those of all CNF-based aerogels and most other relevant carbon-based aerogels reported in literature. We believe that the extraordinary absorption capacities mainly come from the unique honeycomb-like surface pattern and the 3D porous interconnected structure inherited from BC. It has been demonstrated that the spherical SCBC/GE aerogel can be a promising superabsorbent for water environmental protection.

Acknowledgements

This work is supported by the National Natural Science Foundation of China (Grants no. 51172158, 51572187, 51563008) and the Science & Research Foundation of Jiangxi Province (Grant No. 20151BDH80061).

References

1. J. Aurell and B. K. Gullett, *Environ. Sci. Technol.*, 2010, 44, 9431-9437.
2. A. Bayat, S. F. Aghamiri, A. Moheb and G. R. Vakili-Nezhaad, *Chem. Eng. & Technol.*, 2005, 28, 1525-1528.
3. V. Broje and A. A. Keller, *J. Haz. Mater.*, 2007, 148, 136-143.
4. Z.-Y. Wu, C. Li, H.-W. Liang, Y.-N. Zhang, X. Wang, J.-F. Chen and S.-H. Yu,

Sci. Reports, 2014, 4, 1-6.

5. D. Bastani, A. A. Safekordi, A. Alihosseini and V. Taghikhani, *Sep. Pur. Technol.*, 2006, 52, 295-300.
6. M. Zhao and P. Liu, *Desalination*, 2009, 249, 331-336.
7. Q. Zhu, F. Tao and Q. Pan, *ACS Appl. Mater. Interfaces*, 2010, 2, 3141-3146.
8. H. Bi, X. Xie, K. Yin, Y. Zhou, S. Wan, L. He, F. Xu, F. Banhart, L. Sun and R. S. Ruoff, *Adv. Funct. Mater.*, 2012, 22, 4421-4425.
9. H. Bi, Z. Yin, X. Cao, X. Xie, C. Tan, X. Huang, B. Chen, F. Chen, Q. Yang and X. Bu, *Adv. Mater.*, 2013, 25, 5916-5921.
10. S. Park, S.-O. Kang, E. Jung, S. Park and H. S. Park, *RSC Adv.*, 2014, 4, 899-902.
11. M. A. Fulazzaky and R. Omar, *Clean Techn. Environ. Policy*, 2012, 14, 965-971.
12. D. Mysore, T. Viraraghavan and Y. C. Jin, *J.Resid. Sci. & Technol.*, 2006, 3, 5-14.
13. A. Alihosseini, V. Taghikhani, A. A. Safekordi and D. Bastani, *Int. J. Environ. Sci. Tech.*, 2010, 7, 591-598.
14. M. Shavandi, Z. Haddadian, M. Ismail, N. Abdullah and Z. Abidin, *Water, Air, Soil. Pollut.*, 2012, 223, 4017-4027.
15. A. Li, H.-X. Sun, D.-Z. Tan, W.-J. Fan, S.-H. Wen, X.-J. Qing, G.-X. Li, S.-Y. Li and W.-Q. Deng, *Energy Environ. Sci.*, 2011, 4, 2062-2065.
16. N. T. Cervin, C. Aulin, P. T. Larsson and L. Wagberg, *Cellulose*, 2012, 19,

401-410.

17. J. T. Korhonen, M. Kettunen, R. H. Ras and O. Ikkala, *ACS Appl. Mater. Interfaces*, 2011, 3, 1813-1816.

18. N. Chen and Q. Pan, *ACS Nano*, 2013, 7, 6875-6883.

19. Z. Zhang, G. Sèbe, D. Rentsch, T. Zimmermann and P. Tingaut, *Chem. Mater.*, 2014, 2659–2668.

20. J. Yuan, X. Liu, O. Akbulut, J. Hu, S. L. Suib, J. Kong and F. Stellacci, *Nature Nanotechnol.*, 2008, 3, 332-336.

21. G. Tao, L. Zhang, Z. Hua, Y. Chen, L. Guo, J. Zhang, Z. Shu, J. Gao, H. Chen and W. Wu, *Carbon*, 2014, 66, 547-559.

22. H.-P. Cong, X.-C. Ren, P. Wang and S.-H. Yu, *ACS Nano*, 2012, 6, 2693-2703.

23. H.-W. Liang, Q.-F. Guan, L.-F. Chen, Z. Zhu, W.-J. Zhang and S.-H. Yu, *Angew. Chem. Int. Ed.*, 2012, 51, 5101-5105.

24. X. Gui, H. Li, K. Wang, J. Wei, Y. Jia, Z. Li, L. Fan, A. Cao, H. Zhu and D. Wu, *Acta Mater.*, 2011, 59, 4798-4804.

25. X. Gui, J. Wei, K. Wang, A. Cao, H. Zhu, Y. Jia, Q. Shu and D. Wu, *Adv. Mater.*, 2010, 22, 617-621.

26. S. Ozden, T. N. Narayanan, C. S. Tiwary, P. Dong, A. H. C. Hart, R. Vajta and P. M. Ajayan, *Small*, 2014, 688-693.

27. Y. He, Y. Liu, T. Wu, J. Ma, X. Wang, Q. Gong, W. Kong, F. Xing, Y. Liu and J. Gao, *J. Haz. Mater.*, 2013, 260, 796-805.

28. J. Zhao, W. Ren and H.-M. Cheng, *J. Mater. Chem. A*, 2012, 22, 20197-20202.

29. Z.-Y. Wu, C. Li, H.-W. Liang, J.-F. Chen and S.-H. Yu, *Angew. Chem. Int. Ed*, 2013, 52, 2925-2929.

30. Y. Hu, J. M. Catchmark and E. A. Vogler, *Biomacromolecules*, 2013, 14, 3444-3452.

31. W. Czaja, D. Romanovicz and R. M. Brown, *Cellulose*, 2004, 11, 403-411.

32. X. Dong, J. Chen, Y. Ma, J. Wang, M. B. Chan-Park, X. Liu, L. Wang, W. Huang and P. Chen, *Chem. Commun.*, 2012, 48, 10660-10662.

33. H. Hu, Z. Zhao, Y. Gogotsi and J. Qiu, *Environ. Sci. Technol. Lett.*, 2014, 1, 214-220.

34. B. Chen, Q. Ma, C. Tan, T. T. Lim, L. Huang and H. Zhang, *Small*, 2015, 11, 3319-3336.

35. H. Sun, Z. Xu and C. Gao, *Adv. Mater.*, 2013, 25, 2554-2560.

36. Y. Wang, S. Yadav, T. Heinlein, V. Konjik, H. Breitzke, G. Buntkowsky, J. J. Schneider and K. Zhang, *RSC Adv.*, 2014, 4, 21553-21558.

37. Y. Liu, J. Zhou, E. Zhu, J. Tang, X. Liu and W. Tang, *J. Mater. Chem. C*, 2015, 3, 1011-1017.

38. H. Luo, G. Xiong, Z. Yang, S. R. Raman, H. Si and Y. Wan, *RSC Adv.*, 2014, 4, 14369-14372.

39. H. Si, H. Luo, G. Xiong, Z. Yang, S. R. Raman, R. Guo and Y. Wan, *Macromol. Rapid Commun.*, 2014, 35, 1706-1711.

40. Y. Z. Wan, Y. Huang, C. D. Yuan, S. Raman, Y. Zhu, H. J. Jiang, F. He and C. Gao, *Mater. Sci. Eng. C*, 2007, 27, 855-864.

41. L. Hong, Y. L. Wang, S. R. Jia, Y. Huang, C. Gao and Y. Z. Wan, *Mater. Lett.*, 2006, 60, 1710-1713.

42. C. Tokoh, K. Takabe, M. Fujita and H. Saiki, *Cellulose*, 1998, 5, 249-261.

43. T. Kuila, S. Bose, A. K. Mishra, P. Khanra, N. H. Kim and J. H. Lee, *Progress in Materials Science*, 2012, 57, 1061-1105.

44. H.-B. Zhang, W.-G. Zheng, Q. Yan, Y. Yang, J.-W. Wang, Z.-H. Lu, G.-Y. Ji and Z.-Z. Yu, *Polymer*, 2010, 51, 1191-1196.

45. H.-P. Cong, P. Wang and S.-H. Yu, *Chem. Mater.*, 2013, 25, 3357.

46. Y. Xu, W. Hong, H. Bai, C. Li and G. Shi, *Carbon*, 2009, 47, 3538.

47. M. Kačuráková, A. C. Smith, M. J. Gidley and R. H. Wilson, *Carbohydr. Res.*, 2002, 337, 1145-1153.

48. Y. Zhao, C. Hu, Y. Hu, H. Cheng, G. Shi and L. Qu, *Angew. Chem. Int. Ed.*, 2012, 51, 11371-11375.

49. K. H. Kim, Y. Oh and M. Islam, *Nature Nanotechnol.*, 2012, 7, 562-566.

50. J. Li, J. Li, H. Meng, S. Xie, B. Zhang, L. Li, H. Ma, J. Zhang and M. Yu, *J. Mater. Chem. A*, 2014, 2, 2934-2941.

51. C. Gao, Y. Wan, C. Yang, K. Dai, T. Tang, H. Luo and J. Wang, *J. Porous Mater.*, 2011, 18, 139-145.

Figure captions

Fig. 1 Surface images of (a) BC, (b) SBC, (c) CBC, (d) SCBC, (e) SBC/GE, and (f) SCBC/GE.

Fig. 2 SEM images of (a) BC, (b) CBC, (c) SBC, (d) SCBC, (e) SBC/GE, and (f) SCBC/GE.

Fig. 3 XRD patterns of various aerogels.

Fig. 4 FTIR spectra of various aerogels.

Fig. 5 Water contact angles of various aerogels.

Fig. 6 Porosity of CBC, SCBC, and SCBC/GE.

Fig. 7 Specific surface area of CBC, SCBC, and SCBC/GE.

Fig. 8 Compressive load–strain curves of SCBC and SCBC/GE.

Fig. 9 The sequential photographs of SCBC/GE absorbing Sudan III-dyed gasoline oil (a-d) and phenoxin (e-h) and absorption capacities of CBC, SCBC and SCBC/GE aerogels for various organic liquids (i).

Fig. 10 Proposed mechanisms showing the absorption process of liquids into the SCBC/GE.

Fig. 1.

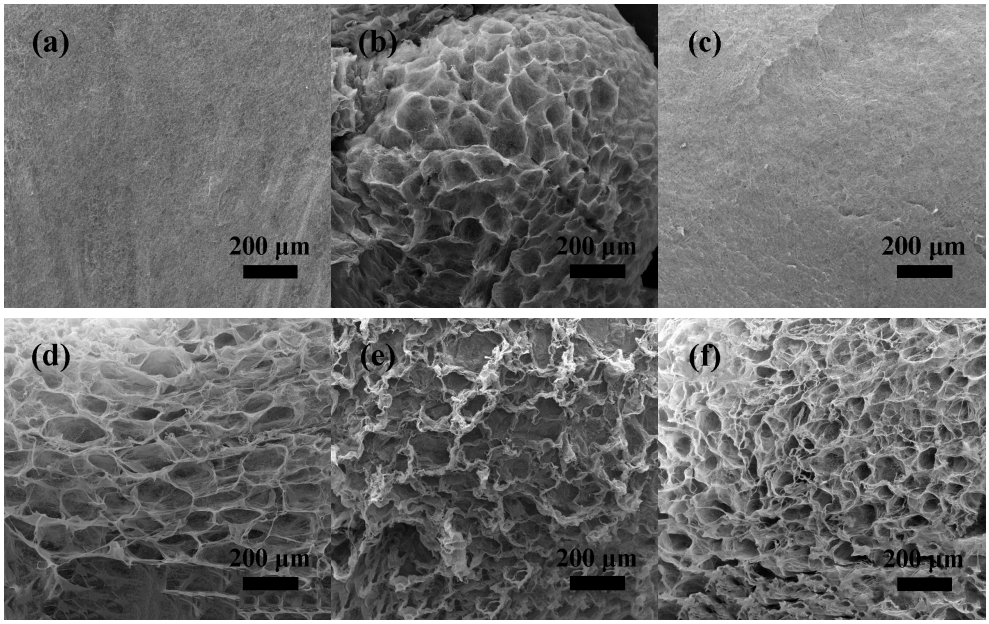

Fig. 2.

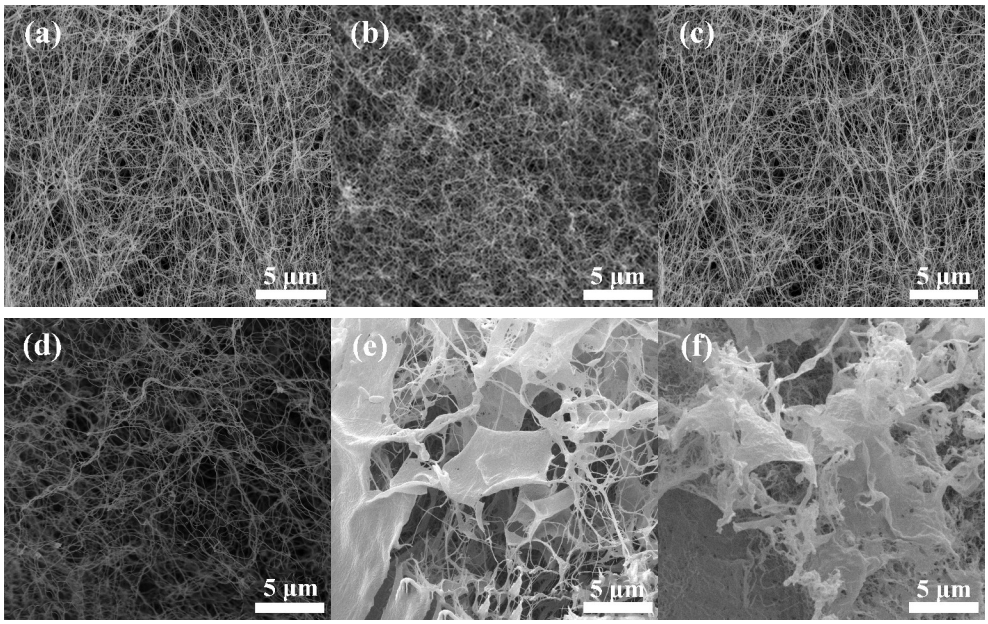

Fig. 3.

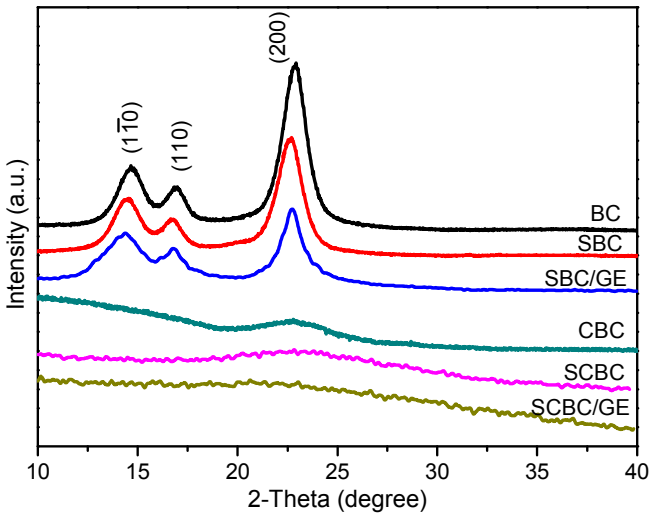

Fig. 4.

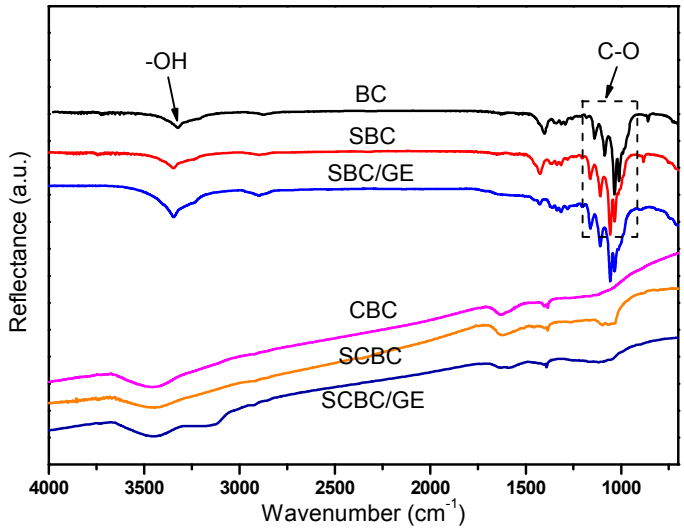

Fig. 5.

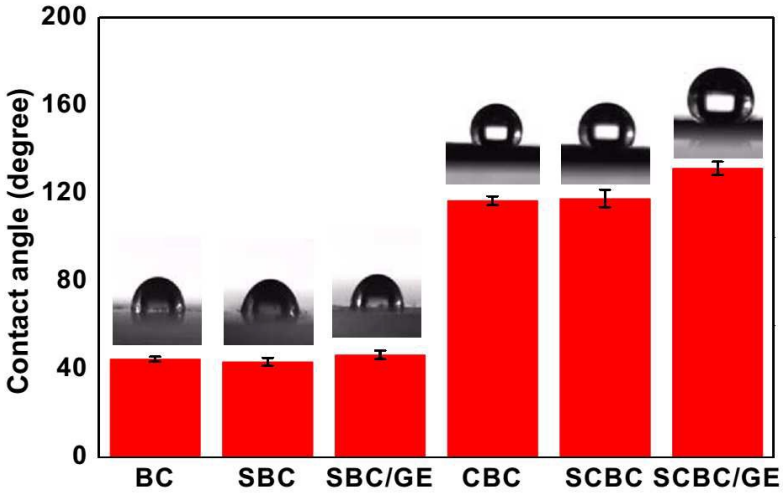

Fig. 6.

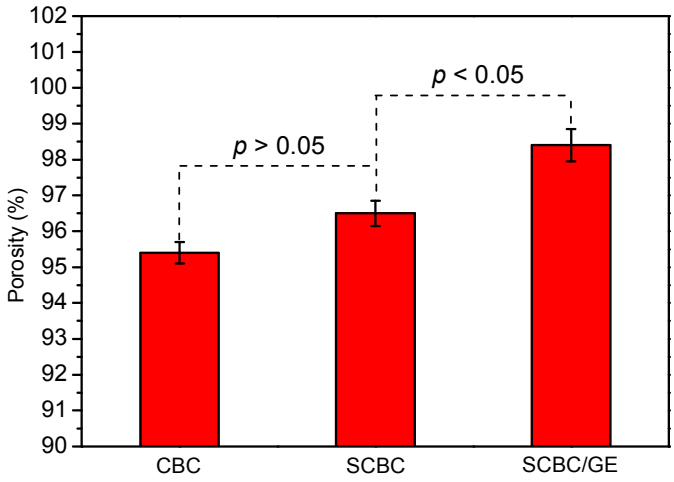

Fig. 7.

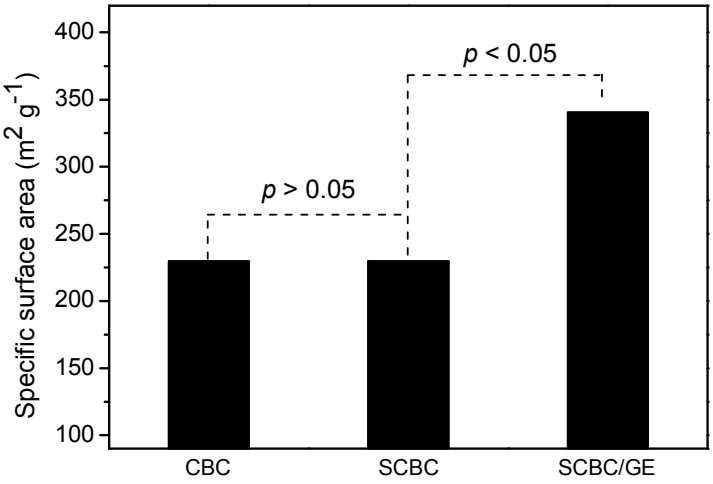

Fig. 8.

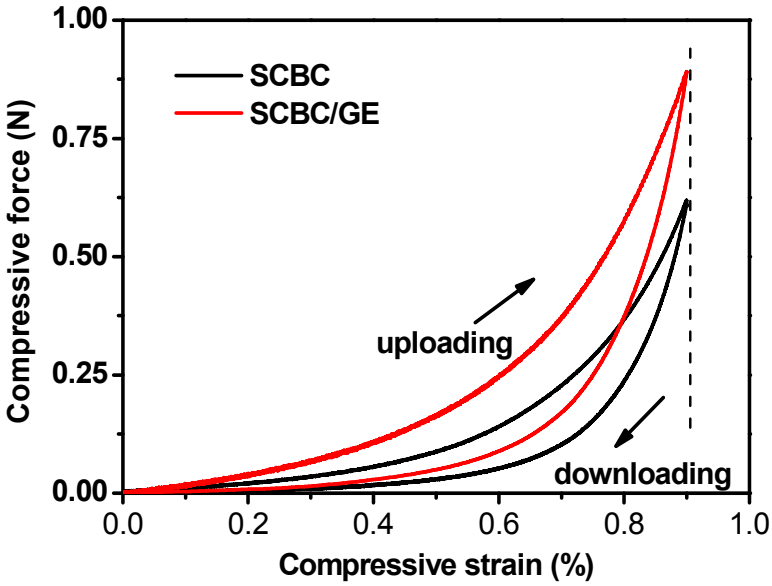

Fig. 9.

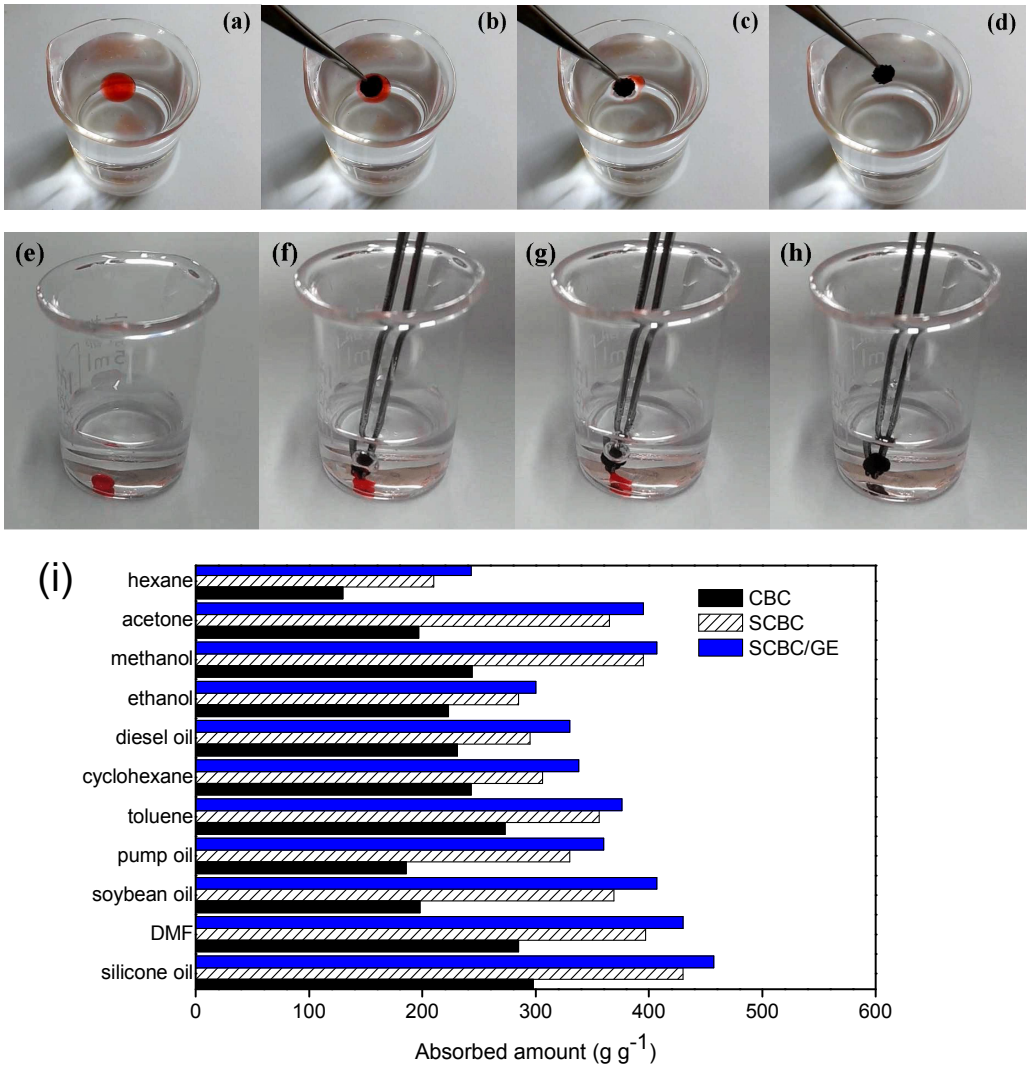

Fig. 10.

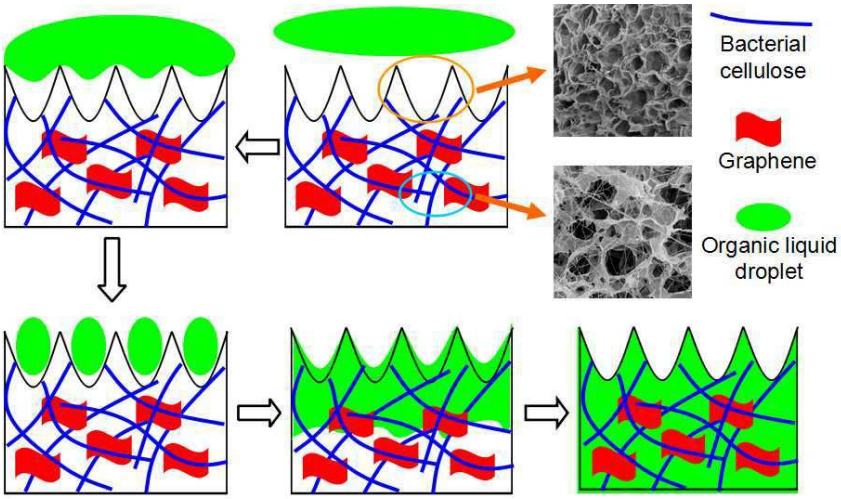

A novel sphere-like carbonized bacterial cellulose/graphene nanocomposite with honeycomb-like surface morphology and three-dimensional (3D) porous structure was synthesized via a facile and scalable one-pot in situ biosynthesis route and carbonization.